

PHOTOMETRY OF EXTENDED SOURCES

G. de Vaucouleurs
The University of Texas
Austin, Texas 78712

As a contribution to the continuing struggle for precision and reliability in photographic surface photometry with Schmidt telescopes the following sections review some of the main sources of errors and ways to avoid them, where possible.

1. ACCIDENTAL AND SYSTEMATIC ERRORS

The following sources of error will be particularly discussed:

- (a) photographic calibration and local errors, microphotometer errors, sky level errors; zero point and integration errors;
- (b) instrumental and atmospheric convolution effects, including the structure of the point spread function (PSF), effects of internal reflections in the corrector and the influence of scattered light (aureole);
- (c) galactic and extragalactic effects, including interstellar extinction and diffuse nebulosities at high latitudes, bright field stars and galaxies; statistical fluctuations in the distribution of sub-threshold stars and galaxies.

2. PHOTOGRAPHIC AND CALIBRATION ERRORS

The luminosity distribution $I(x,y)$ derived from the plate density matrix $D(x,y)$ is affected by errors in the photographic calibration curve $I = f(D)$ and, at low I levels, by errors in the adopted "blank sky" level. The latter is usually determined by polynomial interpolation using "numerical mapping" techniques (Jones *et al.* 1967, Barbon *et al.* 1976, Okamura 1977).

- (a) External calibration. Tube sensitometers, penumbra sensitometers, step wedges and other calibration devices are often poorly designed or implemented, improperly standardized or incorrectly used. In particular, the calibration spots are often much too close to the plate edge; most Schmidt cameras suffer from this defect. Processing irregularities are largest at the edge of the plate; the outermost 2-3 cm should never be

used for calibration. The spots should be spaced widely enough (at least several millimeters) that scattered light from the high intensity steps will not contaminate the low intensity steps or the plate background in their vicinity.

(b) Internal calibration. It is often the case, particularly for some of the older Schmidt plate collections, such as the POSS, that no external calibration scale is available. In such cases, it is possible to construct a characteristic curve by combining the density profiles $D(r)$ of several stars whose magnitudes (or differences δm) are known (Kormendy 1973; Kormendy and Bahcall 1974). This internal calibration is possible because all stars have the same relative intensity profile (point spread function), $I(r)/I(0)$, so that $D(I)$ can be derived by a point-by-point comparison of two or more $D(r)$ profiles of known δm (Figure 1). To work well this method requires that adjacency effects (Eberhard, Kostinsky effects) be negligible, which can be achieved by pushing the development to (or close to) γ_∞ . Otherwise, the characteristic curve derived from stars would not be applicable to extended sources, because adjacency effects vary with the steepness of the density gradient in the image. Consequently, this internal calibration method works better with the soft star images given by long-focus reflectors than with the sharp images given by short-focus Schmidt cameras. An alternative and preferable method in the latter case is to use standard galaxies having precisely known luminosity profiles; one such standard galaxy is NGC 3379 (de Vaucouleurs and Capaccioli 1979) which can be used also to check calibration procedures. Another galaxy usable as a luminosity distribution standard is NGC 4486 (M87) (de Vaucouleurs and Nieto 1978, 1979). There is a need for more standard galaxies well-distributed around the sky.

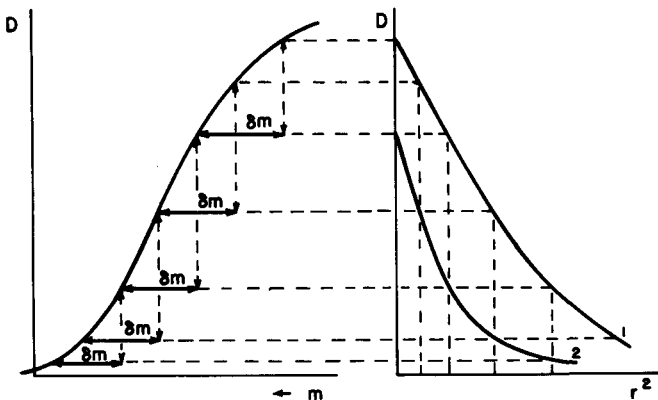
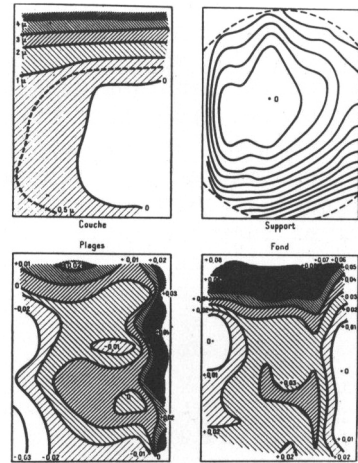


Figure 1
Internal calibration:
derivation of characteristic curve $D(m)$ from density profiles $D(r^2)$ of two stars of known magnitude difference δm .

(c) Photographic emulsions and processing techniques introduce photometric irregularities or "local errors" (de Vaucouleurs 1943, 1945, 1946, 1948c, 1976) whose origin is poorly understood. Processing should be as uniform as possible; if brush development is not practical for large plates, at least the performance of the developing machine on uniformly exposed plates should be checked. Ditto for the drying. Local errors

Figure 2

Local errors: comparison of variations of thickness of emulsion ("couche") (a), departures from flatness of plate ("support") (b), density (above fog) of spots exposed to uniform illumination ("plages") (c), and density variations of plate fog ("fond") (d). Note correlation between (a) and (d), and absence of correlation between (c) and all others (de Vaucouleurs 1946).



are not random errors (noise) on a given plate and so can be mapped and, to a large extent, corrected by interpolation (Figure 2), but they vary from plate to plate in an uncorrelated fashion, so that on the average the differential error increases approximately as the square root of the separation in the plane of the emulsion (random walk). The photometric errors resulting from the local errors in density vary with density (Figure 3). The optimum range is the lower part of the H & D curve (not its inflection point). Procedures for the correction of local errors by interpolation between a network of control spots (de Vaucouleurs 1943, 1946) or by the related technique of "grid photography" (Davis *et al.* 1980) have been developed and are essential to achieve the potential precision of photographic photometry (0.1% under laboratory conditions, 0.5% under astronomical conditions; see de Vaucouleurs 1948d). Under normal conditions interpolation of the sky background by numerical mapping techniques (Jones *et al.* 1967) will serve the same purpose more simply, but at some loss of precision.

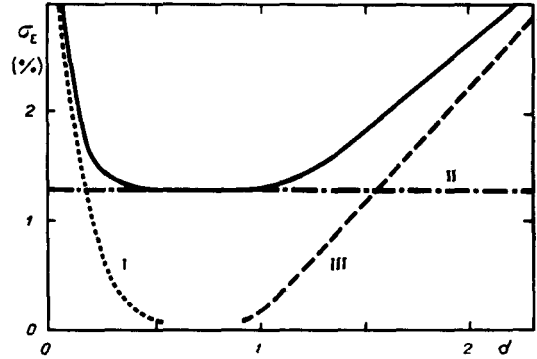
(d) Vignetting. Clearly the vignetting function must be taken into account. This is done automatically when the local sky background determined by interpolation is used as a unit of specific intensity since all fluxes are reduced in the same proportion. However, allowance must be made for apparent changes of the vignetting function due to variable desensitization by water vapor trapped in the air space between filter and plate holder (Dawe and Metcalfe 1982). This effect can be eliminated by nitrogen-flushing (Figure 4).

3. MICROPHOTOMETER AND SKY LEVEL ERRORS

(a) Significant random and systematic errors are often introduced by the microphotometer or densitometer used to measure the plates. This is especially frequent for the common type of uncompensated single beam

Figure 3

Local errors: average photometric errors of spots exposed to uniform illumination as a function of density. Note three components: (I) at low densities microphotometer and plate errors are dominant because of low gradient of characteristic curve, (II) at intermediate densities processing errors are dominant, (III) at high densities non-uniform thickness of emulsion makes increasing contribution. The optimum region is at the base of the linear part of the characteristic curve, not near its inflection point (de Vaucouleurs 1946).



instruments whose readings depend directly on the stability of the light source and of the electronic amplifiers, both notorious for their drift properties. The high speed digitized instruments, such as the PDS machine add to these defects high noise at high densities, a non-linear (or non-logarithmic) response, sensitivity to scattered light, and other sources of error (Bozyan and Opal 1983). It is not uncommon that densities measured on two different days on the same plate even with identical instrumental settings will not repeat precisely, unless special precautions are taken to monitor the response of the instrument. If available, the dual beam, compensated systems are much to be preferred.

(b) All nebular photometry is, per force, done in the presence of a superimposed strong noise signal, the luminosity of the night sky, I_s , so that, for example, the galaxy signal (specific intensity), I_g , is obtained as the difference, $I_g = I_{g+s} - I_s$, between the measured intensity, I_{g+s} , of galaxy + sky and the intensity of the local sky light, I_s , the sum of the airglow, the zodiacal light, and atmospheric and instrumental scattering. This local "sky level" can only be estimated by interpolation across the object field between adjacent "blank sky" areas surrounding it. This interpolation is generally performed by fitting a low-order mapping polynomial in x, y which necessarily assumes a smooth underlying distribution of I_s . High spatial frequency random fluctuations can not be detected or avoided.

At high intensities, when $I_g \gg I_s$, small departures from the interpolating surface have only a minor effect on I_g . For example, if the error in the interpolated sky level is $\delta I_s / I_s \approx 0.01$, the relative error is a negligible 0.1% = 0.001 mag where $I_g = 10 I_s$, or $\mu_g(B) \approx 19.8$ mss (\approx mag per square arc second) if $\mu_g(B) \approx 22.3$ mss. However, in the faint outer parts of a galaxy where $I_g \ll I_s$ and where $D_{g+s} - D_s$ tends asymptotically to zero the error becomes dominant; thus, if $I_g = 0.1 I_s$, or

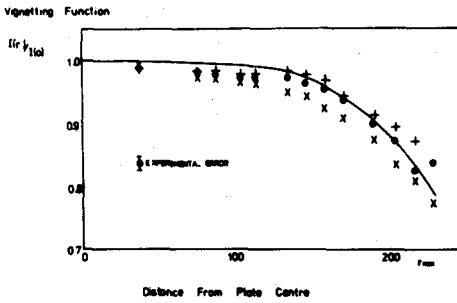


Figure 4
 Vignetting: apparent vignetting functions for UK 1.2 m Schmidt telescope. Line: comparison plates (geometric effects and scattering); +: hypersensitized plates without filter, no N₂-flushing of plateholder; x: hypersensitized plates with filter, no N₂-flushing of plateholder; o: hypersensitized plates with filter and N₂-flushing of plateholder (Dawe and Metcalfe 1982).

$\mu_S(B) \approx 24.8$ mss, the same 1% error in I_g introduces an error of 10% or 0.1 mss in I_g , and if $I_g = 0.01 I_S$, or $\mu_g(B) \approx 27.3$, $\delta I_g/I_g \approx 1$ and the magnitude error diverges. This effect can drastically change the apparent photometric profile of the faint outer coronae of galaxies (Figure 5). In particular, it can introduce fictitious "tidal radii" truncations or, conversely, "tidal extensions" to elliptical galaxies, depending on whether the sky level is placed slightly too high or too low. In the best case, current photoelectric techniques define the sky level with mean errors of $\sim 0.1\%$ (equivalent to $\mu_B \approx 30$ mss), but photographically it is difficult to do better than 0.5% ($\mu_B \approx 28$ mss) on single plates.

4. ZERO POINT AND INTEGRATION ERRORS

The zero point is usually fixed by photoelectric photometry, either by direct photoelectric scans calibrated versus standard stars, or by equating the photographic luminosity integral to the flux measured photoelectrically within the corresponding integration area, generally a circular aperture centered at the nucleus in the case of galaxies. In either case the following errors may be present:

(a) Zero point errors. The zero point of the magnitude scale is affected by errors in the magnitudes of the standard stars, in the calibration of the amplifier in the d.c. mode (or improper resolution corrections in the pulse counting mode) and in the transformation equations to the standard system. The possibility of error in measuring the diameters (or areas) of the field apertures and in the plate scale used to transform them to angular measure should not be ignored. Both should always be checked by timing transits of polar stars. In most cases, it is difficult to reduce the total mean error of the zero point from all sources to less than 0.02-0.03 mag.

(b) Integration errors. These are introduced by errors in the adopted sky level, by the finite width of the integration intervals, by inclusion of field stars or background galaxies. In the case of NGC 3379 (de Vaucouleurs and Capaccioli 1979), the total mean error (zero point and

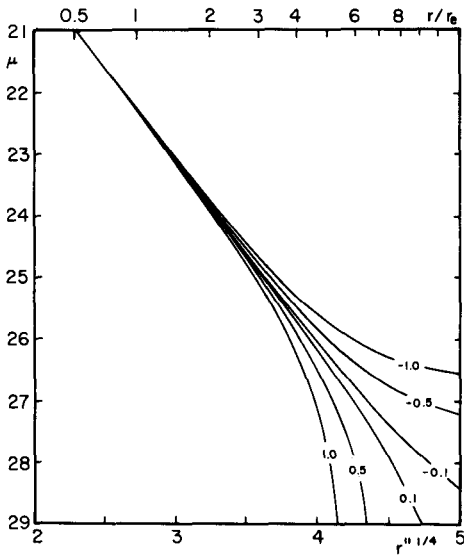


Figure 5
Effect of errors in adopted sky level on apparent luminosity profile of an EO galaxy obeying the r^{-4} law. Note that depending on its sign the systematic error δD_s (in units of 0.01 when $D_s = 0.8$) introduces an apparent "tidal cutoff" or a "tidal extension". Surface brightness scale μ and radial scale r are for NGC 3379 (Capaccioli and de Vaucouleurs 1983).

integration) of photoelectric aperture photometry by several observers was 0.065 mag, much larger than is generally quoted by individual observers from internal evidence, but in line with the rule of thumb that on the average true external mean errors are 2-3 times larger than internal errors.

(c) Extrapolation errors. In the absence of systematic errors in the photometry the integrated magnitude of a diffuse object, such as a galaxy, that fades insensibly into the night airglow, the calculated integrated magnitude within a specified isophote, refers unavoidable to some unknown fraction of the total luminosity of the galaxy. Procedures for the derivation of the total (or asymptotic) magnitude have been developed (de Vaucouleurs 1948b, 1977); the incompleteness correction is often in the range of 0.3 to 0.03 mag, depending on the detection threshold.

5. INSTRUMENTAL AND ATMOSPHERIC CONVOLUTION EFFECTS

Because of their small plate scale, Schmidt telescopes in general are not suitable for high-resolution studies of small structures, such as the nuclei of galaxies, particularly if coarse-grained photographic emulsions are used. However, if wide field electronographic cameras can be successfully adapted for use with Schmidt cameras, as proposed by Griboval (this conference), and especially if such systems can be operated in space, the enormous gain in resolving power will make them surpass the resolution presently available at the Cassegrain foci of large ground-based reflectors. Then the same problems of convolution by the instrumental point spread function (PSF) will need to be considered.

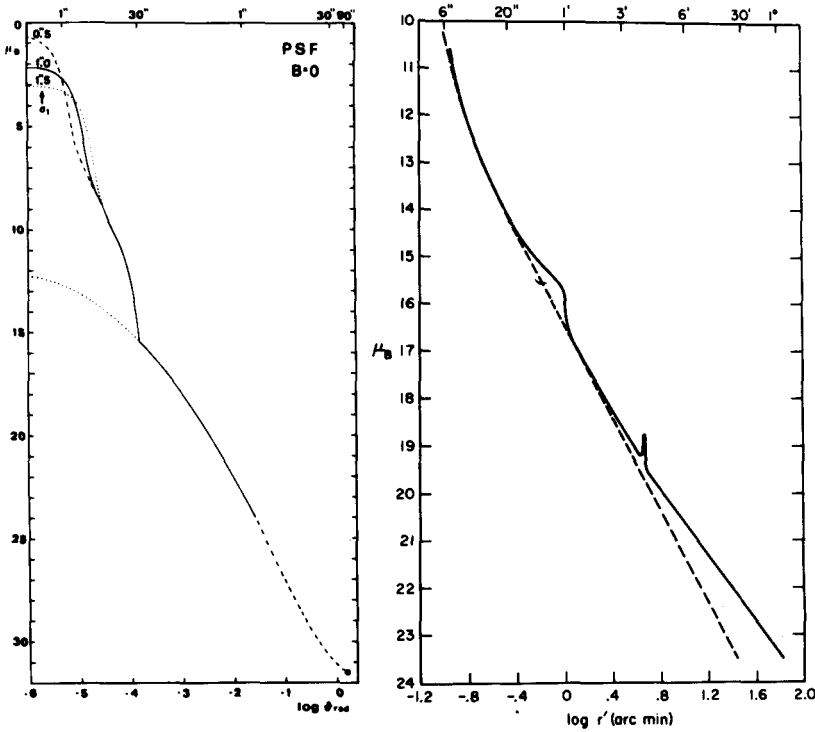


Figure 6

Typical point spread functions for (a) McDonald reflectors after Capaccioli and de Vaucouleurs (1983) and (b) Palomar 1.2 m Schmidt telescope after Kormendy (1973). Note effects of variable seeing in (a), of internal reflections and halation in (b). Surface brightness scales are normalized to star of total magnitude $B = 0$.

(a) Point Spread Functions. A combination of high-resolution microphotometric analysis of stellar images of different magnitudes, and of photoelectric scans of very bright stars gives the typical PSF of medium sized reflectors at ~ 2 km elevation shown in Figure 6a. This may be compared with the mean PSF for the Palomar 1.2 m Schmidt telescope (Figure 6b); except for the effect of multiple internal reflections and the lack of high resolution data in the center of Figure 6b, the curves are generally similar. Two distinct regimes are in evidence: (I) a steep decline, extending typically to $r \approx 30''$, is dominated by telescopic diffraction and atmospheric turbulence; this is the "image" proper; (II) a shallower decline extending out to $r \approx 1.5'$, dominated by distant telescopic and atmospheric (particle) scattering, may be described as the "aureole" (Dermendjian 1957, 1959). The latter eventually merges smoothly into the Rayleigh scattering component (dashed line in Figure 6a). Under average seeing conditions the total range of surface brightness is ~ 30 magnitudes.

The innermost part of the image which is dominated by atmospheric turbulence does not have a fixed profile but varies with seeing conditions. In general, the core of the image is well-approximated by a Gauss function (de Vaucouleurs 1948b; King 1971; Brown 1978) $G_1(r; \sigma_1)$ which includes something like 80 to 90% of the energy in the star image (component I). Beyond a few seconds from the center of the image the wings are brighter than expected from G_1 alone. This excess, which can be represented by the sum of gaussians (Brown 1978) or exponentials (Newell 1980), contains typically ~ 10 to 20% of the energy in the image. This fraction varies with the condition of the optics and the turbidity of the atmosphere (Piccirillo 1973).

(b) Effect of scattered light (aureole). Beyond $r \approx 30''$ the PSF is dominated by scattered light forming an "aureole" around the central image (Figure 6a). Within the "image" the contribution of the aureole to the observed surface brightness is essentially negligible; for example, at the center the aureole is roughly 10 magnitudes fainter than the image. But the contribution of the aureole to the observed surface brightness of the outer parts of a galaxy may become increasingly significant at distances $r > 30''$, depending on the luminosity law in the object and the scaling factor. An example is given in Figure 7.

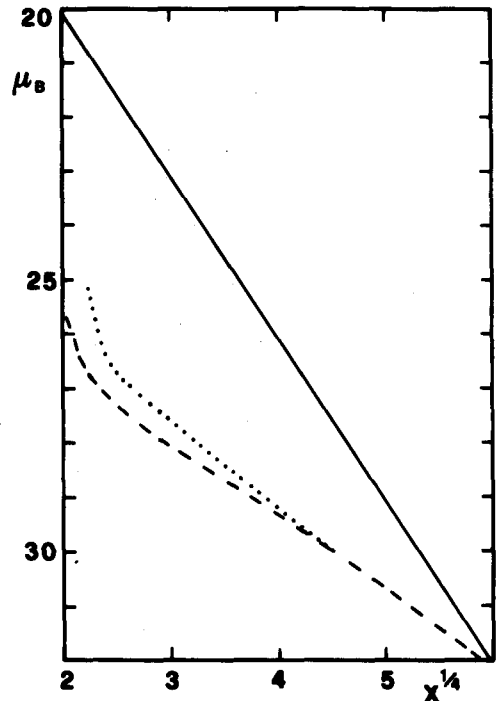


Figure 7
Scattered light (dashed curve) of model of NGC 3379 (solid line) and of central point source having the same total magnitude (dotted curve) for the PSF of Figure 6a. Note that luminosity excess due to scattered light is less than 0.14 mss at all $x > 459''$ where $\mu_B(\text{obs.}) > 28.0$ (Capaccioli and de Vaucouleurs 1983).

6. GALACTIC AND EXTRAGALACTIC EFFECTS

External galaxies are observed through the irregularly absorbing and scattering interstellar dust layer, among the field stars and (at least in clusters) among other galaxies, which cause more or less random fluctuations in the luminosity distribution in the galaxy image and in the sky "background." Galactic nebulosities are similarly observed against a foreground and background of other nebulosities, stars and the pervading interstellar medium. Further, undetected (sub-threshold) stars and galaxies cause additional fluctuations in the "blank sky" level.

(a) Galactic extinction effects at high latitudes. While it may be assumed that galactic extinction is uniform over the small areas covered by most galaxies on large scale reflector plates, this assumption is not warranted in the case of the larger fields covered by Schmidt plates nor in the case of large galaxies at low galactic latitudes, such as M31 and the Magellanic Clouds. While the assumption of zero extinction within 30 to 40 degrees from the galactic poles is demonstrably untenable (de Vaucouleurs and Buta 1983), and the cosec b law is definitely valid (statistically) up to both galactic poles, it is very difficult to make realistic estimates of the small scale fluctuations of galactic extinction at high latitudes. The most direct evidence comes from the detection of reflection nebulosities.

(b) High-latitude reflection nebulosities. It has been known for many years that faint emission and/or reflection nebulosities can be detected by deep photography at intermediate galactic latitudes (de Vaucouleurs 1955, 1960; King, Taylor and Tritton 1979). Spectacular examples have been detected in recent years thanks to the development of the high-contrast IIIa-J emulsion (Arp and Kormendy 1972, Arp and Lorre 1976, Sandage 1976, Cannon 1979). All fields show much fine filamentary, cirrus-like structure down to the resolution limit ($\sim 2''$) of the 1.2 m Schmidt telescopes. At latitudes $|b| < 45^\circ$ available data indicate a range of surface brightness $27 > \mu_B > 25$ mss in regions where the estimated mean extinction is $A_B \approx 0.3$ mag. At latitude $|b| > 45^\circ$ corresponding information is not yet available, except that the maximum surface brightness is probably much lower, perhaps $\mu_B > 27$ mss and its angular power spectrum is unknown.

Note that only the fluctuations about the mean surface brightness of the foreground sky in a given field introduce errors in galaxy photometry (a uniform veil would not be detected on direct photographs nor would cause errors, but would simply raise the detection threshold). In the case of photographic surface photometry and to the extent that the diffuse galactic component is a continuous function, the lower frequencies of the brightness fluctuations are effectively removed when numerical mapping techniques are used to define the sky "background" density level across the object field.

(c) Bright field stars and galaxies. Each star or galaxy in the field of the telescope is a source of scattered light superimposed on the airglow

and galactic foreground. In principle, this component can be calculated via the PSF as the sum of the convolved images (particularly the aureoles) of all sources in the field. The problem is particularly severe in galaxy clusters where the local sky level is determined to a large extent by the overlapping coronae of individual galaxies and their optical aureoles as well as by the intergalactic stellar "sea" permeating the whole cluster (de Vaucouleurs and de Vaucouleurs 1970, Thuan and Kormendy 1977). Spectacular examples of this problem have been brought out by photographic contrast enhancement techniques (Malin 1981, Malin and Carter 1980).

In the case of detailed photographic surface photometry the major (low frequency) part of the stellar aureole component is automatically removed by numerical mapping of the "sky" background (Capaccioli and D'Odorico 1980). The procedure fails when a bright star is directly superimposed on the image of the galaxy or nebula, in which case there is no satisfactory way of restoring the lost information.

(d) Sub-threshold stars and galaxies. As was first noted by Miller (1963) statistical fluctuations in the number density of stars and galaxies which are individually below the detection threshold introduce another type of noise which may be significant and impose still another limit to the precision of the photometry at faint light levels. The first and second moments of the contributions of subthreshold stars and galaxies to the luminosity of the "blank sky" near the galactic poles have been calculated by numerical integration of their respective luminosity functions under the assumption of Poisson statistics (i.e. ignoring clustering). An application to photoelectric scans of NGC 3379 (Capaccioli and de Vaucouleurs 1983) shows that (i) the contributions to the total noise of the stars and galaxies fainter than $B \approx 20.5$ are very nearly equal, (ii) the major contributors to the noise in each case are the stars and galaxies within one magnitude of the detection threshold, and (iii) the total noise due to subthreshold stars and galaxies is equivalent to $\mu_B \approx 29.8$ mss.

7. CONCLUSIONS

The various sources of accidental and systematic errors in photographic (and photoelectric) surface photometry of faint extended sources, particularly galaxies, are such that it is difficult, if not impossible, to obtain significant quantitative information at brightness levels fainter than $\mu_B \approx 28$ mss ($\Sigma < 0.3 \Sigma_{\odot} \text{pc}^{-2}$). Even at brighter levels errors less than 0.1 mag are difficult to achieve and in the nuclear regions ($\mu_B < 18$ mss) larger errors are introduced by convolution effects. Most of these errors are inherent to the nature of things, and except for improved resolution and lower sky background with space telescopes, will not be easily reduced by future technical advances.

This review paper, based mainly on work done in collaboration with Prof. M. Capaccioli, was supported in part by NSF Grant INT 8022847 and CNR Grant 100601C under the US-Italy Cooperative Science Program.

REFERENCES

- Arp, H. and Kormendy, J. 1972, *Astrophys. J. Letters* 178, L101.
- Arp, H. and Lorre, J. 1976, *Astrophys. J.* 210, 58.
- Barbon, R., Benacchio, L. and Capaccioli, M. 1976, *Mem. Soc. Astr. Italiana* 47, 263.
- Bozayan, E.P. and Opal, C.B. 1983, preprint.
- Brown, G.S. 1978, *Univ. Texas Publ. Astr. No.* 11.
- Cannon, R.D. 1979, in D.S. Evans (ed.), *Photometry, Kinematics and Dynamics of Galaxies*, Dept. Astr., Univ. Texas, Austin, p.27.
- Capaccioli, M. and de Vaucouleurs, G. 1983, *Astrophys. J. Suppl.* 52,
- Capaccioli, M. and D'Odorico, S. 1980, in P.L. Bernacca and R. Ruffini (eds.), *Astrophysics from Spacelab*, D. Reidel Publishing Company, Dordrecht, p.317.
- Davis, M., Feigelson, E. and Latham, D.W. 1980, *Astr. J.* 85, 131.
- Dawe, J.A. and Metcalfe, N. 1982, *Proc. Australian Soc. Astr.* 4, 466.
- Dermendjian, D. 1957, *Ann. Geophys.* 13, 286; 1959, *Ann. Geophys.* 15, 218.
- de Vaucouleurs, G. 1943, *Sci. Industries Photog.* (2), 14, 149; 1945, *J. Physique* (8), 6, 205; 1946, *Sci. Industries Photog.* (2), 17, 257; 1948a, *J. des Observateurs* 31, 113; 1948b, *Ann. d'Astrophys.* 11, 247; 1948c, *Revue d'Optique* 27, 541; 1948d, *Com. Nat. Fr. Astr., Comm. et Mem.*, 160; 1955, *Observatory* 75, 170; 1958, *Astrophys. J.* 128, 465; 1960, *Observatory* 80, 106; 1976, in J.L. Heudier (ed.), *I.A.U. Working Group on Photographic Problems*, Proc. Grenoble meeting, p. 93; 1977, *Astrophys. J. Suppl.* 33, 211.
- de Vaucouleurs, G. and Buta, R. 1983, *Astr. J.* 88, 939.
- de Vaucouleurs, G. and Capaccioli, M. 1979, *Astrophys. J. Suppl.* 40, 699.
- de Vaucouleurs, G. and de Vaucouleurs, A. 1970, *Astrophys. Letters* 5, 219.
- de Vaucouleurs, G. and Nieto, J.L. 1978, *Astrophys. J.* 220, 449; 1979, *Astrophys. J.* 230, 697.
- Griboval, P. 1984, these proceedings.
- Jones, W.B., Obitts, D.L., Gallet, R.M. and de Vaucouleurs, G. 1967, *Publ. Dept. Astr., Univ. Texas, Ser. II, Vol. I., No.* 8.
- King, D.F., Taylor, K.N.R. and Tritton, K.P. 1979, *Monthly Notices Roy. Astron. Soc.* 188, 719.
- King, I. 1971, *Publ. Astr. Soc. Pacific* 83, 199.
- Kormendy, J. 1973, *Astr. J.* 78, 255.
- Kormendy, J. and Bahcall, J.N. 1974, *Astron. J.* 79, 671.
- Malin, D.F. 1978, *Nature* 276, 591; 1981, *Amer. Astron. Soc. Photo-Bulletin No.* 27, 4.
- Malin, D.F. and Carter, D. 1980, *Nature* 285, 643.
- Miller, R.H. 1963, *Astrophys. J.* 137, 733.
- Newell, E.B. 1980, in G. Sedmak, M. Capaccioli and R. Allen (eds.), *Image Processing in Astronomy*, Osservatorio Astr., Trieste, p. 100.
- Okamura, S. 1977, *Ann. Tokyo Astr. Observ., Vol. XVI, No.* 3, p.11.
- Piccirillo, J. 1973, *Publ. Astr. Soc. Pacific* 85, 278.
- Sandage, A.R. 1976, *Astr. J.* 81, 954.
- Thuan, T.X. and Kormendy, J. 1977, *Publ. Astr. Soc. Pacific* 89, 466.